Fundamental Research 5 (2025) 602–611

Contents lists available at ScienceDirect

Fundamental Research

journal homepage: http://www.keaipublishing.com/en/journals/fundamental-research/

Article

Terahertz photoneuromodulation of lateral orbitofrontal cortex neurons ameliorates stress-induced depression and cognitive impairment

Yuanyuan He[a,b,c,#], Jing Ma[b,#], Yun Yu[b,#], Junkai Yin[b], Ge Gao[d], Yifang Yuan[b], Hao Ruan[b], Xueqing Yan[a,*], Zihua Song[b,*], Chao Chang[a,b,*]

[a] State Key Laboratory of NPT, and Key Laboratory of HEDP of MoE, CAPT, Peking University, Beijing 100871, China
[b] Innovation Laboratory of Terahertz Biophysics, National Innovation Institute of Defense Technology, Beijing 100071, China
[c] School of Safety Engineering, North China Institute of Science and Technology, Hebei 065201, China
[d] School of Life Science, Tsinghua University, Beijing 100084, China

ARTICLE INFO

Article history:
Received 8 July 2024
Received in revised form 6 December 2024
Accepted 9 December 2024
Available online 19 December 2024

Keywords:
Terahertz photoneuromodulation
Depression
Cognitive impairment
Orbitofrontal cortex
Selective serotonin reuptake inhibitors

ABSTRACT

Depression imposes a staggering global socioeconomic burden. Current pharmacotherapies face major limitations, including slow efficacy, adverse effects, and non-response rates of up to 55%, necessitating novel therapeutic modalities. This study introduces terahertz (THz) photoneuromodulation as an innovative physical intervention for depression, offering several advantages over conventional pharmacological or optogenetic approaches. Mild THz photoneuromodulation circumvents the need for exogenous agents or genetic modifications, mitigating potential risks while precisely modulating neurotransmitter levels and neuronal excitability to alleviate depression-like behaviors. In a chronic restraint stress (CRS) mouse model, THz photostimulation rapidly attenuated hyperactivity and increased serotonin levels by 107.5% ± 45.3% in lateral orbitofrontal cortex glutamatergic neurons (OFC^{Glu}) compared to those treated with antidepressants. This led to marked improvements in depressive-like behaviors and cognitive function. Furthermore, THz modulation of OFC activity recapitulated the effects of chemogenetic inhibition, underscoring the OFC's pivotal role in regulating depressive states. This research unveils THz photoneuromodulation as a promising, safe, rapid-acting, and durable neurotherapeutic strategy addressing persistent unmet needs in depression treatment.

1. Introduction

Major depressive disorder (MDD) is characterized by notable deficits in executive function, memory, and attention, often accompanied by persistent cognitive deficits [1,2]. Depression is a prominent factor in the development and deterioration of comorbidities, including Alzheimer's disease, diabetes, and autoimmune disorders [1]. The World Health Organization (WHO) has recognized it as a substantial contributor to the global disease burden and a leading cause of disability and mortality [3].

In the face of increasingly competitive social environments, chronic stress has emerged as a significant risk factor for depression, with prevalence rates steadily rising [4–6]. Recent research has identified the orbitofrontal cortex (OFC) as a promising therapeutic target for psychiatric disorders, including depression [7]. The OFC plays a crucial role in emotion processing and reward value assessment, maintaining reciprocal connections with key brain regions such as the amygdala, ventral striatum, insula, and cingulate cortex [8–11]. A prevailing theory posits that the lateral OFC (lOFC) contributes to depression through heightened responsiveness to the absence of expected rewards, while reduced reward responsiveness in medial OFC (mOFC) may lead to anhedonia [12,13]. This is supported by studies showing increased OFC activity during negative and depressed mood states, with remission linked to decreased OFC activity [14–16].

Conventional antidepressants, particularly selective serotonin reuptake inhibitors (SSRIs), have shown efficacy in alleviating negative bias in emotional information processing by modulating OFC activity [17,18]. However, these standard pharmacological interventions face significant limitations, including slow onset of action and potential adverse effects [19,20]. Additionally, a substantial proportion of patients (6–55%) remain unresponsive to these standard treatments [21–25], highlighting the urgent need for alternative therapeutic approaches. Brain stimulation therapies have emerged as promising alternatives for modulating neural activity in specific brain regions. Deep brain stimulation (DBS) [26] and repetitive transcranial magnetic stimulation (rTMS) [27,28] targeting the OFC have demonstrated notable antidepressant

* Corresponding authors.
E-mail addresses: x.yan@pku.edu.cn (X. Yan), szh2016@mail.ustc.edu.cn (Z. Song), gwyzlzssb@pku.edu.cn (C. Chang).
# These authors contributed equally to this work.

https://doi.org/10.1016/j.fmre.2024.12.004

effects. In particular, TMS of lOFC has shown benefits in depressed patients who are unresponsive to the dorsomedial and lateral prefrontal cortex TMS [28], establishing lOFC as a crucial target area for brain stimulation therapy in depression.

Recent advances in electromagnetic stimulation have identified terahertz (THz) photons, electromagnetic waves between the microwave and infrared regions of the spectrum [29,30], as a promising therapeutic tool. These waves have demonstrated significant effects on neurobiological regulation, including modulation of neuronal excitability, neurotransmitter activity [31], synaptic plasticity [32], and animal behavior [33]. While THz stimulation (THz-S) holds promise as a novel brain stimulation technique to treat neuropathic disorders. Despite these promising findings, the specific role of THz in regulating lOFC neural activity and its potential in mitigating depression remains to be fully explored.

In this study, we investigate how THz at specific frequencies modulates lOFC neurons and affects chronic restraint stress (CRS)-induced depression-like behaviors and cognitive impairments. Our findings demonstrate that brief THz-S resulted in a reduction in the action potential frequency of OFC^{Glu}, while concurrently elevating the action potential threshold current. Notably, neural activity remained suppressed even up to 6 min after cessation of the irradiation. Moreover, compared to antidepressants (SSRIs, Paroxetine), THz irradiation of the OFC in CRS mice resulted in more than a twofold increase in serotonin (5-HT) levels, with a rise of 107.5% ± 45.3%. In addition, THz-S significantly ameliorated depression-like behavior in CRS mice, as evidenced by increased central-region residence time in the open field test. In the tail suspension test and forced swimming test, immobility time was reduced by 64.3% ± 8.9% and 44.8% ± 10.8%, respectively. The Barnes maze and novel object recognition experiments showed that THz exposure significantly alleviated cognitive impairments in CRS mice.

These findings indicate that, in comparison to SSRIs, THz therapy offers faster modulation of electrical activity in OFC neurons, greater up-regulation of 5-HT levels, and longer-lasting antidepressant effects, thereby presenting a novel approach for treating depression.

2. Materials and methods

2.1. Animals

Male C57BL/6 J mice (procured from SiPeiFu Biotechnology Co., Ltd), aged 8–10 weeks and weighing approximately 25 g, were used in the experiments. Mice were housed under controlled conditions with a 12-h light/dark cycle, ad libitum access to standard chow and water, and were group-housed (4–5 per cage) at an ambient temperature of 23–25 ˚C. The experimental groups were assigned using randomization. All animal procedures were approved by the Institutional Animal Care and Use Committee at Tsinghua University.

2.2. Whole-cell patch-clamp recordings

Mice were deeply anesthetized with isoflurane and decapitated for brain extraction. The brain was affixed to a bedplate in a vibrating microtome (VT1200s, Leica). Coronal slices (180 μm) were sectioned at 0.18 mm s^{-1} in ice-cold, oxygenated (95% O_2/5% CO_2) artificial cerebrospinal fluid (ACSF) containing (in mM): 2.4 $CaCl_2$, 3 KCl, 129 NaCl, 20 $NaHCO_3$, 1.3 $MgSO_4$, 1.2 KH_2PO_4, 3 HEPES, and 10 glucose. Slices were recovered in oxygenated ACSF at 33–35 ˚C for 30–60 min.

For electrophysiological recordings, slices were transferred to a submerged recording chamber superfused with oxygenated ACSF (2.5–3 mL/min, 25 ˚C) maintained by an online heater (TC-344B, Warner Instrument). The ACSF was adjusted to pH 7.3–7.4 and 300–305 mOsm/L. Whole-cell patch-clamp recordings were performed on OFC neurons visualized using a 40 × water-immersion lens (BX51WI, Olympus) and an infrared-CCD camera. The intracellular solution contained (in mM): 130 K-gluconate, 5 KCl, 2 $MgCl_2$, 0.6 EGTA, 10 HEPES, 2 Mg-ATP, and 0.3 Na-GTP, and 0.1% biocytin (B4261, Sigma), adjusted to pH 7.2 and 285–290 mOsm/L. Signals were amplified (MultiClamp 700B), filtered at 2.8 kHz, and digitized at 10 kHz.

2.3. Biocytin-glutamate co-labeling staining

Following action potential recordings, neurons were maintained in whole-cell configuration to facilitate biocytin diffusion from the recording electrode into the cell. To ensure adequate biocytin labeling, recordings were maintained for a minimum of 10 min. The recording electrode was then slowly withdrawn to preserve cellular integrity. Brain slices were subsequently fixed in 4% paraformaldehyde at 4 ˚C for 24 h. Tissue sections were blocked with 5% bovine serum albumin (BSA) and 0.5% Triton X-100 for 2 h at room temperature. The sections were then incubated with anti-glutamate primary antibody (1: 200, rabbit, G6642, Sigma) at 4 ˚C for 48 h. Following primary antibody incubation, sections were treated with 594-labeled streptavidin (1: 200, S11227, Thermo Fisher) at 4 ˚C for 24 h under light-protected conditions. After three washes with PBST (Phosphate-Buffered Saline with Tween 20), the sections were incubated with donkey anti-rabbit secondary antibody conjugated with Alexa Fluor 488 (1: 200, A-21206, Invitrogen) for 2 h at room temperature in darkness. Nuclear counterstaining was performed using 4,6-diamidino-2-phenylindole (DAPI; 1: 2000, Sigma) for 3 min.

2.4. Stereotaxic surgery

Mice were deeply anesthetized with 1%–2% isoflurane in oxygen (flow rate: 0.4–0.6 L/min) and mounted on a stereotaxic frame (RWD, Shenzhen, China). Following hair removal, the cranial surface was disinfected with iodophor and a surgical incision was made in the scalp to expose the skull. The skull surface was leveled according to the OFC brain region coordinates (anteroposterior [AP], 2.4 mm; mediolateral [ML], 1.5 mm; dorsoventral [DV], 1.35 mm), and holes were drilled bilaterally in the skull. The body temperature of these mice was maintained at 36 ˚C with a heating pad.

Bilateral cannula were buried in OFC with the following specifications: cannula diameter 450 μm, bilateral spacing 3 mm, cannula cap height 7.8 mm, and catheter length 3 mm. The catheter was inserted into the above two skull holes. The cannula was fixed on the skull surface with dental cement, the scalp was glued together with tissue glue, and the wound was disinfected with iodophor.

2.5. Chemogenetic manipulation

Mice were deeply anesthetized with 1%–2% isoflurane in oxygen and mounted on a stereotaxic frame. A 200 nL volume of viruses (rAAV-CaMKIIα-hM4Di-mCherry or rAAV-CaMKIIα-mCherry [Brain-VTA, Wuhan, China]) was injected into the OFC using a fine glass micropipette with a tip diameter of 10–15 μm connected to a 10 μL syringe (Hamilton, USA). The injection speed and volume were controlled using a micro-infusion pump (micro4, WPI). The injection speed was 30 nL/min. A total of 200 nL of the virus was delivered to each site, and the pipette was left in place for at least 10 min after the injection before being slowly withdrawn to avoid virus back-flow. The scalp was sutured using a suture needle and thread and disinfected with iodophor. Behavioral tests and electrophysiological recordings were performed at least three weeks after the viral injection. Clozapine-N-oxide (CNO) (MCE, Monmouth Junction, NJ, USA) was dissolved in 0.9% saline to 1 mg/mL and injected (5 mg/kg, i.p.) 30 min before behavior tests.

2.6. Light source and THz photon irradiation

During in vitro brain slices irradiation, the stimulation parameter (frequency 34 THz, pulse duration 0.5 μs, repetition rate 200 kHz, duty cycle 10%) was controlled using a quantum cascade mid-infrared laser

(Daylight solution Inc., model MIR cat). The fiber (diameter: 400 μm, NA = 0.30 ± 0.03, IRF-S-9, IRflex) was affixed to the robotic arm of a micromanipulator and moved through the micromanipulator to position itself above the brain slice near the OFC. At this point, a glass electrode was manipulated using another micromanipulator to clamp onto OFC neurons for electrophysiological recording.

In the vivo experiments, the laser used was a 34-THz QCL (frequency 34 THz, pulse duration 2 μs, repetition rate 200 kHz, duty cycle 40%). Mice were deeply anesthetized with 1%–2% isoflurane in oxygen and mounted on a stereotaxic frame for in vivo irradiation. The catheter cap was removed, and the fiber (diameter: 240 μm, NA = 0.30 ± 0.03, IRF-S-9, IRflex) was inserted into the buried catheter with the locator at a depth of 10.8 mm (starting point above the catheter) precisely targeted to OFC region. The THz irradiation protocol for in vivo biosafety assessment and treatment is 10 min/day for 3 consecutive days.

2.7. Animal models and behavioral testing procedures

Mice were subjected to periodic immobilization by confinement within a fixator for 6 h daily over 21 days. Control mice were allowed unrestricted movement within their cages, but were without access to food or water during this period. The fixator was cleaned after each restraint session to eliminate potential confounding factors. Mice were given two days of rest following CRS before anatomical and electrophysiological assessments to minimize acute stress effects.

All behavioral tests were conducted on the same cohort of mice, with specific time intervals between tests to minimize potential carryover effects. The testing sequence was as follows: open field test (Day 0); novel object recognition (Days 0–1, consisting of habituation and testing); Barnes maze (Days 3–6: three days of training followed by probe test); tail suspension test (Day 9); forced swimming test (Day 11).

2.8. Open field test

Before the experiments, experimental mice were acclimatized for approximately 2 h in a learning laboratory to minimize stress levels. During the experiment, each mouse was placed individually in the center of an open field measuring 40 cm × 40 cm × 40 cm and allowed to explore freely for 5 min while their movements were recorded using a behavior recorder. The central area of the instrument, measuring 24 cm × 24 cm, was designated for analysis. The Smart v3.0 software was utilized to analyze offline the time taken by mice to enter this area and their total travel distance.

2.9. Tail suspension test

The mouse tail was secured approximately 1 cm from its tip and suspended 50 cm above the ground for 5 min during the experiment. The experimental procedure was videotaped from a lateral perspective, with the total immobility time of the mouse during this period being recorded. Initial movements were considered stationary, while passive swaying motions were considered as immobility.

2.10. Forced swimming test

A fresh water-filled clear glass cylinder (height: 30 cm, diameter: 19 cm) was prepared with the water level set at 25 cm from the bottom. The mice were placed in the cylinder and filmed from a lateral view for 5 min to record their immobility time. Despair behavior was defined as floating on the water's surface while making minimal movements to keep their noses above it.

2.11. Barnes maze

Prior to behavioral testing, mice underwent a 2-hour habituation period in the behavioral laboratory to minimize stress. The Barnes maze consisted of a circular platform with 20 equidistant holes along the perimeter, with an escape box (target) positioned beneath one hole. The day before training, each mouse was habituated to the escape box for 4 min.

Training was conducted across two consecutive days, with three daily trials per mouse. Each trial terminated upon either escape box entry or after a 4-minute cutoff. Between trials, the maze was rotated while maintaining the relative spatial position of the target hole and sanitized with 75% ethanol to eliminate olfactory cues.

Testing was performed following the training phase, comprising three trials under identical protocol conditions. Performance metrics included escape latency (time to locate target) and error count (number of incorrect hole investigations, defined as nose-pokes or forepaw entries into non-target holes). Values were averaged across the three trials for statistical analysis.

2.12. Novel object recognition test

Prior to testing, mice were habituated to the behavioral laboratory for 2 h to minimize stress. The Novel object recognition test consisted of three sequential phases with standardized intervals.

In the habituation phase (Stage 1), each mouse was individually placed in an open-field arena (40 cm × 40 cm × 40 cm) for 5–10 min/day for 2 consecutive days of free exploration. Following a 10-minute intertrial interval in the home cage, the familiarization phase (Stage 2) commenced, where two identical objects (A and B) were positioned 10 cm from opposing corners. Mice were allowed 5 min to explore both objects. After a 1-hour retention interval, the test phase (Stage 3) was conducted, where object B was replaced with a novel object (C), while object A remained in its original position. Mice were again given 5 min for exploration.

Object exploration was defined as nose-directed behavior within 2 cm of the object. The exploration time for novel (t1) and familiar (t2) objects was recorded, and the discrimination ratio was calculated as DR% = [t1/(t1 + t2)] × 100%. Between trials, all objects and the arena were cleaned with 75% ethanol to eliminate olfactory cues.

2.13. Enzyme-linked immunosorbent assay (ELISA)

The enzyme-linked immunosorbent assay based on a two-antibody one-step sandwich method was used. Samples, standard substances, and horseradish peroxidase (HRP)-labeled detection antibodies were added into the micropores pre-coated with dopamine (DA) and 5-HT antibodies, incubated, and washed. The color was created using the substrate TMB, which was converted to blue by peroxidase catalysis and yellow by acid. The color depth was positively correlated with the amounts of neurotransmitters detected in the brain. The optical density was measured at 450 nm wavelength with an enzyme label. The difference between a change of 5-HT concentration in THz-exposed CRS mice (a) and that in PRXT-treated CRS mice (b) was calculated as: (a – b)/b × 100%, $a = (C_{CRS+THz} - C_{CRS})/ C_{CRS} \times 100\%$, $b = (C_{CRS+PRXT} - C_{CRS})/ C_{CRS} \times 100\%$.

2.14. HE staining

Hematoxylin-eosin (HE) was performed to evaluate the effects of THz on OFC brain tissue. The standard staining procedures included dewaxing the tissues in water, staining with HE, dehydration with gradient alcohol, clearing with xylene, and sealing with neutral gum.

2.15. Immunofluorescence

Mice were deeply anesthetized with pentobarbital (20 mg/kg) and transcardially perfused with 0.9% saline followed by 4% paraformaldehyde (PFA) in 0.1 M phosphate buffer. Brains were post-fixed in 4%

PFA at 4 °C for 24 h, then cryoprotected in sequential 20% and 30% sucrose solutions at 4 °C until tissue sank. Coronal sections (40 μm) were obtained using a cryostat (Leica CM1860, Germany) and stored at −20 °C in cryoprotectant solution (30% glycerin, 20% ethylene glycol in PBS).

For immunofluorescence staining, sections were washed in PBS (3 × 5 min) and incubated in permeabilization/blocking solution (0.5% Triton X-100, 5% BSA in PBS) for 2 h at room temperature. Sections were then incubated with anti-heat shock protein70 primary antibody (1: 200, rabbit, BES-18921PA, BIOESN) in blocking buffer (0.3% Triton X-100, 3% BSA in PBS) at 4 °C for 24 h. Following PBS washes (3 × 5 min), sections were incubated with Alexa Fluor 594-conjugated goat anti-rabbit secondary antibody (1: 400, 111–585–003, Jackson) for 2 h at room temperature. After final PBS washes (3 × 5 min), sections were counterstained with DAPI and mounted using an anti-fade mounting medium.

2.16. Statistical analysis

The data were analyzed using GraphPad Prism, Fiji ImageJ and Clampfit (Axon pClamp software), and results were presented as the mean ± SEM. Action potential firing frequency was analyzed using two-way repeated measures ANOVA with post hoc comparisons. The paired Student's *t*-test was used to analyze rheobase and action potential waveforms before, during, and after THz irradiation. Unpaired Student's *t*-test was used to compare other data. Statistical significance was accepted using the following criteria: $^{*}p < 0.05$, $^{**}p < 0.01$, $^{***}p < 0.001$, n.s. (not significant). No statistical methods were used to predetermine sample sizes.

3. Results

3.1. Terahertz radiation modulates excitability of glutamatergic neurons in the lateral orbitofrontal cortex (lOFC^{Glu})

We selected the terahertz frequency band of 30–45 THz due to its low water absorption but strong biomolecular absorption properties [34], with approximately 34 THz previously shown to exert regulatory effects on the nervous system [35]. Using a power density of 60 mW/mm^2 at the laser fiber tip, we conducted whole-cell current-clamp recordings from acute mouse OFC slices to assess the impact of THz-S on neuronal excitability (Fig. 1a).

Our results demonstrated that THz-S significantly decreased the frequency of action potentials and increased the threshold current in lOFC neurons (Fig. 1b-d). This inhibitory effect persisted for at least 6 min post-irradiation. In contrast, when the lOFC region was irradiated with 465 nm blue light, no significant changes in neural excitability were observed (Fig. S1). Importantly, THz-S at 60 mW/mm^2-THz-S did not induce significant alterations in neuronal membrane potential (Fig. 1e), suggesting a minimal impact on the overall neuronal state. Further analysis revealed that THz-S significantly reduced the half-wave width of action potentials and increased their decay slope, without affecting the rising slope, amplitude, or threshold. These findings imply that the THz-induced decrease in OFC neuronal excitability may be attributed to enhanced potassium channel conductance (Fig. S2), consistent with previous reports [36]. Using biocytin labeling and glutamate immunofluorescence co-localization, we confirmed that the recorded neurons were indeed OFC glutamatergic neurons (OFC^{Glu}) (Fig. 1f). In summary, 60 mW/mm^2-THz-S can effectively modulate lOFC^{Glu} neuronal excitability through enhanced potassium channel conductance, while maintaining a favorable safety profile.

To investigate the dose-dependency of THz effects, we examined the impact of lower intensity (44 mW/mm^2) THz radiation on OFC^{Glu} neurons. Although this intensity significantly decreased neuronal firing frequency during the 2- and 4-minute exposure periods, the effect was not sustained post-exposure (Fig. S3a). Moreover, no significant change in threshold current was observed (Fig. S3b). These results indicate that a higher intensity of THz-S (60 mW/mm^2) is required for rapid and sustained inhibition of OFC neurons.

3.2. Biosafety profile of terahertz irradiation in vivo

Similar to infrared and microwaves, THz waves are readily absorbed by polar molecules, such as water, resulting in spatial weakening of energy distribution and noticeable thermal effects, including potential heat damage [37]. To compensate for the energy absorption of THz by brain tissue and to achieve an effective irradiation range, we increased the power density of THz to 166 mW/mm^2 in vivo. However, increasing the power density also raises the irradiation temperature, which may pose a risk of tissue damage.

To address biosafety concerns associated with THz radiation in vivo, we conducted a comprehensive evaluation of its thermal effects and potential risks at tissue levels. Using a temperature sensor in an artificial cerebrospinal fluid (ACSF) bath, we measured temperature changes with exposures to 166 mW/mm^2-THz radiation in two dimensions (Fig. 2a). The results showed minimal thermal effects, with maximum temperature increases remaining below 1.5 °C at distances of 0 μm from the fiber along the Y-axis (Fig. 2b).

For in vivo safety assessment, we implanted bilateral catheters near the lOFC of mice using stereotactic techniques. Three days post-surgery, the mice were exposed to THz radiation (166 mW/mm^2 or 332 mW/mm^2) for three days (10 minutes per day). We then examined the expression of heat shock protein 70 (HSP70), a sensitive marker of thermal stress, in OFC brain tissue following THz irradiation. Immunofluorescence analysis revealed that while 332 mW/mm^2-THz significantly increased HSP70 expression, the 166 mW/mm^2-THz treatment did not differ from control conditions (Figs. 2c, d). Furthermore, H&E staining demonstrated that only the high-intensity (332 mW/mm^2) THz irradiation elicited an acute inflammatory response (Fig. 2e). Recent studies have shown that frequency-dependent sensory stimulation affects brain barrier permeability and glymphatic flow [38]. In contrast to light-based stimulation, our THz approach at 166 mW/mm^2 shows minimal thermal effects and no inflammatory response, indicating preserved brain barrier integrity and therapeutic potential.

Collectively, these findings indicate that THz intensities of 166 mW/mm^2 and below are within acceptable safety levels for potential therapeutic applications.

3.3. Terahertz intervention ameliorates lOFC^{Glu} neuronal hyperactivity and depressive behaviors in chronic restraint stress (CRS) mice

Given the involvement of lOFC neuronal hyperexcitation in conditions such as depression, obsessive-compulsive disorder, and other mental illnesses [26,39], we sought to assess the regulatory effects of THz irradiation on neuronal activity and behavior in CRS mice model of depression (Fig. 3a). CRS mice exhibit neuronal hyperexcitability in lOFC^{Glu} (Fig. 3b-d), mirroring the imaging findings in depressed patients, along with pronounced depression-like behaviors and cognitive impairments (Fig. S4).

To evaluate the in vivo effects of THz on CRS mice, we implanted bilateral catheters near the lOFC of CRS mice using stereotactic techniques. Three days post-surgery, the mice were exposed to either 166 mW/mm^2-THz or 465 nm blue light for three days (10 minutes per day). Electrophysiological experiments revealed that 166 mW/mm^2-THz irradiation significantly reduced action potential frequency and increased threshold current in lOFC^{Glu} neurons of CRS mice; however, exposure to 465 nm did not result in significant differences (Fig. 3b-d). Behavioral assessments demonstrated robust therapeutic effects of THz exposure in CRS mice relative to their untreated counterparts. THz-treated CRS mice exhibited significantly enhanced exploratory behavior,

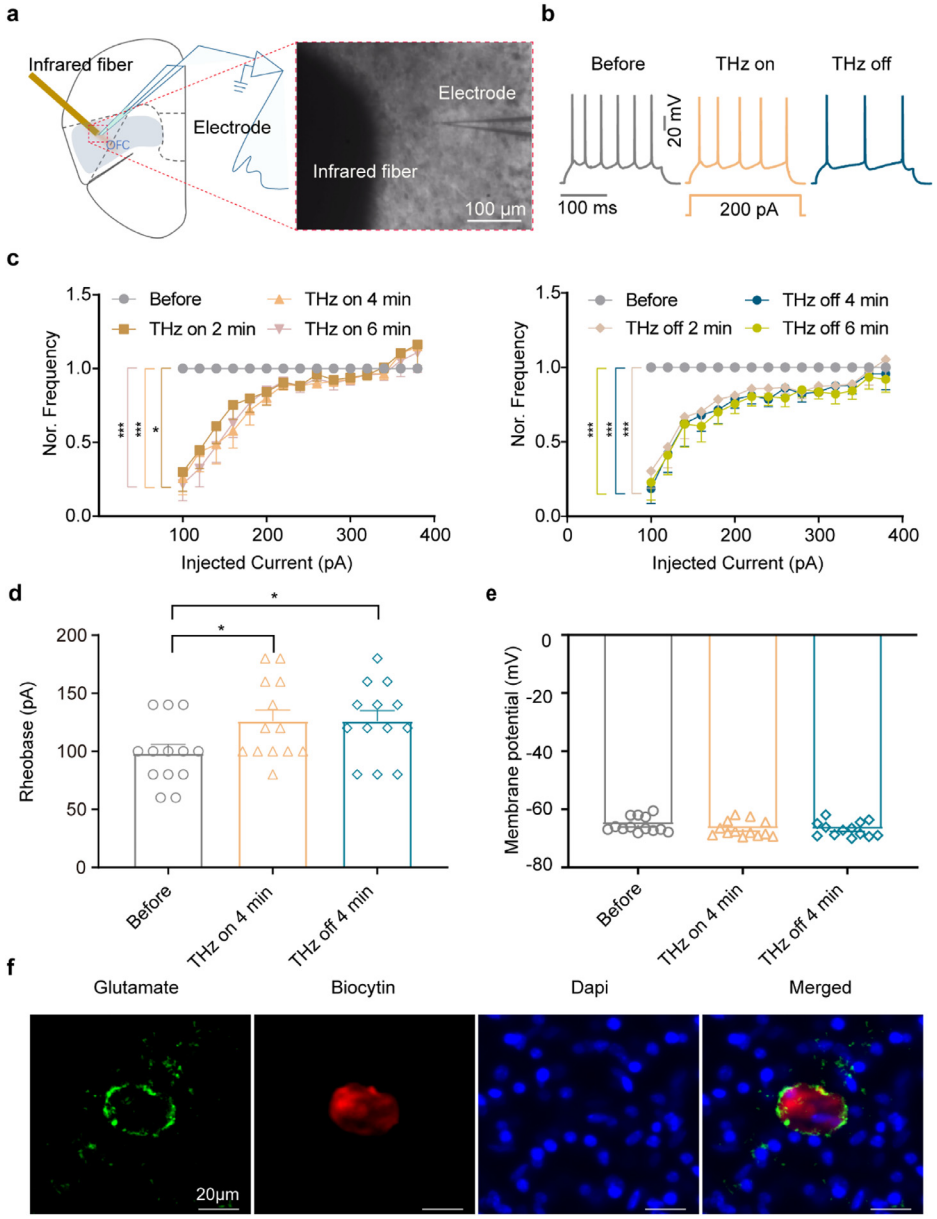

Fig. 1. THz with 60 mW/mm² wave causes changes in vitro OFC^{Glu} neurons. (a) Diagrammatic sketch (left) and real-object picture (scale bars: 100 μm) of the position of infrared fiber and electrode relative on OFC brain region. The gray area is the OFC brain area, where the target area is the lateral OFC (lOFC) (b-e) Representative traces (b) and normalized data of action potentials (c), rheobase (d), and resting membrane potential (e) were recorded from glutamate neurons in OFC slices induced by gradient current (60–380 pA, step 20 pA) before, during and after THz wave exposure. (n = 13 cells from three mice per group). (f) Recording of an lOFC neuron filled with biocytin showing glutamate (scale bars: 20 μm). All data are presented as mean ± SEM. Two-way repeated measures ANOVA with post hoc comparisons for **c** and paired t-test for **d** and **e**: $^{*}p < 0.05$, $^{**}p < 0.01$, $^{***}p < 0.001$.

as evidenced by increased time spent in the central region of the open field (Fig. 3e). Notably, THz exposure substantially reduced despair-like behaviors, with decreased immobility time in both tail suspension (64.3% ± 8.9%) and forced swim tests (44.8% ± 10.8%) (Fig. 3f, g). Cognitive performance also improved markedly, as demonstrated by reduced latency (26.1% ± 5.8%) and fewer errors (33.7% ± 9.4%) in Barnes maze navigation (Fig. 3h). Furthermore, THz stimulation enhanced cognitive flexibility, increasing the novel object discrimination ratio by 26.0% ± 9.7% compared to untreated CRS controls (Fig. 3i). Remarkably, THz-treated CRS mice demonstrated behavioral metrics comparable to non-stressed controls across all assessments (Fig. 3e-i). In contrast, exposure to 465 nm light showed no therapeutic efficacy, with these mice displaying behavioral patterns indistinguishable from untreated CRS controls (Fig. 3e-i).

The OFC is extensively innervated by monoamines [40]. For example, dopamine (DA) neurons from both the ventral tegmental area (VTA) and the dorsal raphe nucleus (DRN) project to the mOFC and lOFC, with greater expression of fibres in the mOFC [41]. The OFC receives intensive 5-HT innervation from the dorsal raphe nucleus and is associated with animals' ability to adapt to unexpected rewarding events in the environment [42]. Both 5-HT and DA play key roles in emotional regulation. Exogenous application of these and other neurotransmitters decreased current-evoked spike firing of lOFC neurons [40]. THz reduces lOFC^{Glu} neuroexcitability and alleviates depression, possibly through increased monoamine neurotransmitter distribution. Importantly, the reciprocal innervation enables the OFC to regulate both its own 5-HT input and 5-HT input to the rest of the forebrain [42]. This regulatory effect of THz on 5-HT levels in the lOFC extends to various OFC regions and

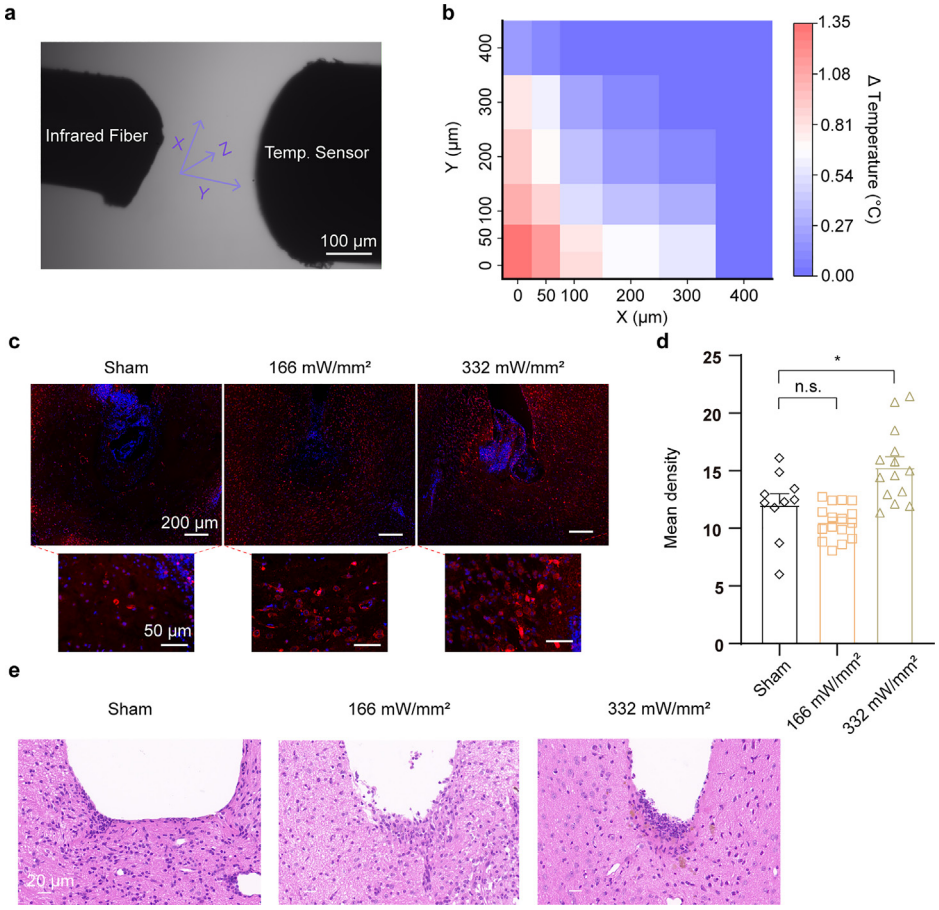

Fig. 2. Biosafety of THz illumination in vitro and in vivo. (a) Real-object picture of the relative position of infrared fiber and temperature sensor, scale bars: 100 μm. (b) A two-dimensional heatmap of temperature change in ACSF. (c, d) Representative image (scale bars: 200 μm and 50 μm) (c) and corresponding statistical plots (d) of expression level of HSP70 under different THz stimulation intensities (n = 10–16 from three mice). (e) Representative pictures of HE staining (scale bars: 20 μm).

the broader forebrain. Our investigation of THz effects on 5-HT and DA projection levels across the OFC showed that THz irradiation increased 5-HT levels by 10.8% ± 7.0% in CRS mice, while DA levels remained unchanged (Fig. 3j and S5). These findings suggest that THz may alleviate depression by inhibiting OFC^{Glu} neuron excitability through 5-HT upregulation in the OFC region. Further research is needed to determine whether this 5-HT upregulation affects other OFC subregions.

To benchmark the efficacy of THz against a standard pharmacological intervention, we compared its effects to those of paroxetine (PRXT, Fig. S6a), an SSRI widely used in clinical practice [43]. PRXT (5 mg/kg, intraperitoneal injected 30 min before testing) was shown to effectively reduce immobility time in C57BL/6 J and C57BL/6 N mice during the forced swimming test [44] and will be used in follow-up trials. Our results demonstrate that both THz and PRXT significantly suppressed OFC neuronal hyperexcitability in CRS mice (threshold current up-regulation: THz 50.8% ± 50.9%, p = 0.0006; PRXT 39.1% ± 28.4%, p = 0.001, Fig. S6b, c), with THz exhibiting a more rapid inhibitory effect (2 min for THz vs. 30 min for PRXT). Additionally, THz induced a larger increase in OFC 5-HT content compared to PRXT (Fig. S6d, THz 10.8% ± 7.0% vs. PRXT 5.2% ± 1.9%, p = 0.03, unpaired Student's t-test). While both interventions significantly alleviated depression and cognitive impairment (Fig. S6e-i), the duration of behavioral improvement was notably longer with THz (approximately 2 weeks) compared to PRXT (0.5–2 hours).

In conclusion, THz irradiation effectively alleviates depression-like behavior and cognitive impairment in CRS mice by upregulating 5-HT release and inhibiting OFC^{Glu} neuronal excitability, exhibiting stronger and more sustained effects compared to PRXT.

3.4. Chemogenetic inhibition of OFC^{Glu} neurons recapitulates the antidepressant effects of THz stimulation

To further validate the mechanistic relationship between reduced OFC excitatory neuronal activity and improvements in depression and cognitive function, we employed a chemogenetic approach to selectively suppress OFC^{Glu} neuronal activity in CRS mice. Chemogenetic inhibition of glutamatergic neurons was technically achieved by locally injecting rAAV-CaMKIIα-hM4Di-mCherry into lOFC. Five days post-surgery, the mice underwent a 21-day chronic restraint stress before subsequent experiments (Fig. 4a). The hM4Di was conditionally expressed in glutamatergic neurons at 4 weeks after intra-lOFC viral micro-injection (Fig. 4b, c). Clozapine N-oxide (CNO), which is a synthetic ligand for human muscarinic engineered receptors, binds and activates hM3Dq and hM4Di for the chemogenetic manipulation of neuronal activity [45]. Whole-cell patch-clamp recordings revealed a reduction in neuronal excitability of glutamatergic neurons after CNO (10 mM) perfusion ex vivo (Fig. 4d, e).

Behavioral tests were conducted 30 min after intraperitoneal injection of CNO (1 mg/mL, 5 μL/g body weight) in CRS mice expressing either hM4Di or mCherry control virus. Compared to mCherry, hM4Di-expressing CRS mice showed: increased time spent in the central area during the open field test (Fig. 4f), reduced immobility in both the tail

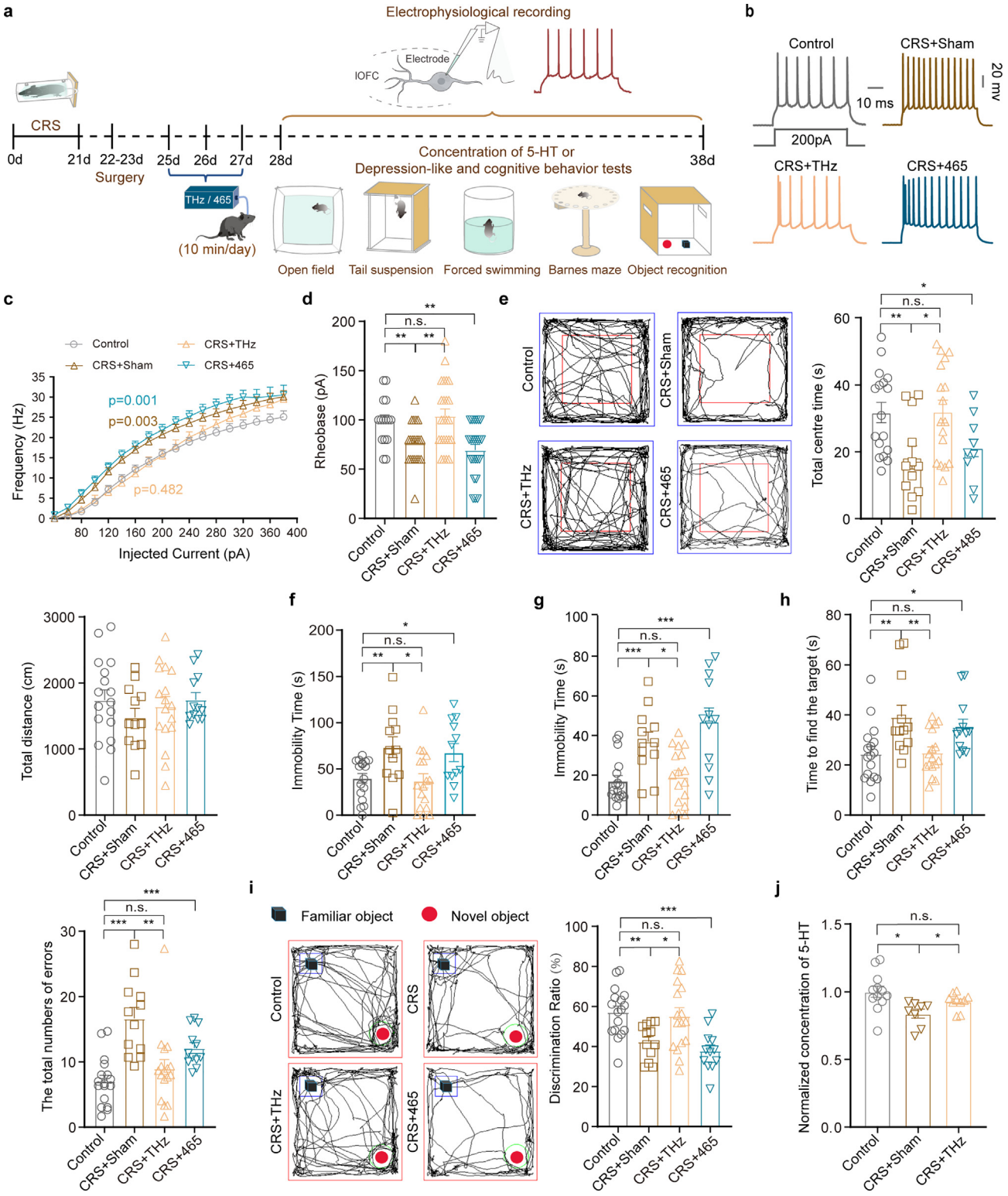

Fig. 3. Effects of 166 mW/mm² THz radiation on lOFCGlu neuronal activity and behavior in CRS mice. (a) Overall scheme for THz to regulate neuronal activity and behavior in CRS mice. The experiments included 4 groups: Control (untreated mice), CRS+Sham (CRS mice with implanted bilateral cannulae), CRS+THz (CRS mice exposed to THz radiation), CRS+465 (CRS mice exposed to 465 nm blue light). (b-d) Representative traces of action potentials (APs) (b), frequency of APs (induced by 0–380 pA, step 20 pA) (c) and rheobase (d) were recorded from glutamatergic neurons in the lOFC from different groups (n = 15–24 neurons from four mice per group). (e-i) Regulation of depressed and cognitive impairment behaviors by THz or 465 nm blue light in CRS mice (n = 12–17), including the open field test (representative movement trajectory and statistical data) (e), tail suspension test (f), forced swimming test (g), Barnes maze (h), and novel object recognition test (representative track plots and statistical data) (i). (j) Regulation of 5-HT concentration in OFC neurons by THz for CRS mice (n = 8–12). All data are presented as mean ± SEM. The significance was assessed using two-way repeated measures ANOVA with post hoc comparisons in c, unpaired t-test in d-j. $^{*}p < 0.05$, $^{**}p < 0.01$, $^{***}p < 0.001$, n.s. (not significant).

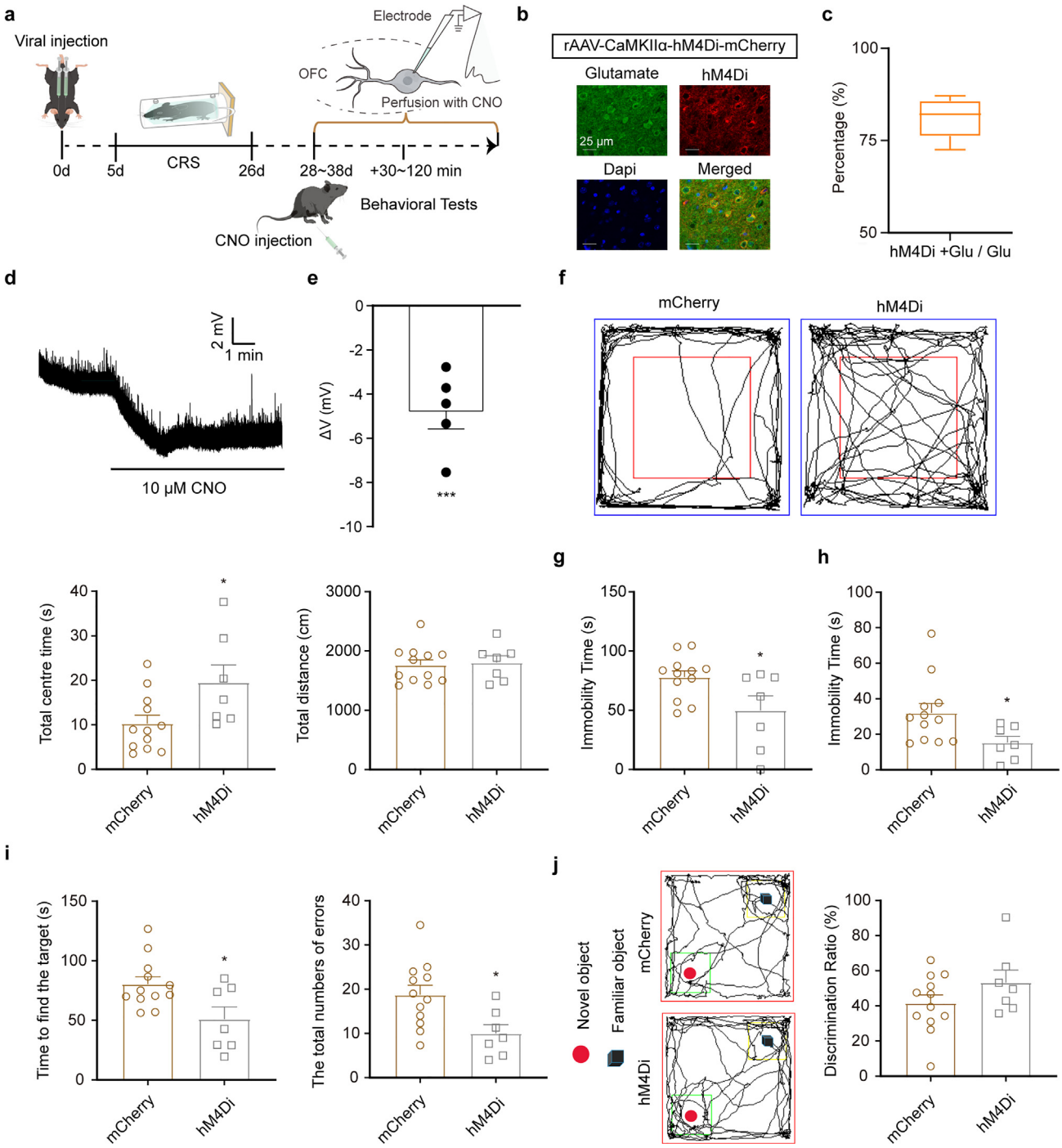

Fig. 4. Chemogenetic inhibition of lOFC^{Glu} neurons alleviates depression-like and cognitive impairment behaviors in CRS mice. (a) Schematic of viral injection, Clozapine-N-oxide (CNO) administration, and experiments. (b) Representative imaging of hM4Di viral expression within glutamatergic neurons in the lOFC after viral injection. Scale bars: 25 μm. (c) Percentage of glutamate co-labeled with hM4Di in total glutamate (n = 6 slices from three mice). (d, e) Representative trace (d) and statistics (e) show that the bath application of CNO (10 μM) hyperpolarizes glutamatergic neurons (n = 5 slices from three mice). (f-j) Changes in depression-like behaviors and cognitive impairment, including the open field test (representative movement trajectory and statistical data) (f), tail suspension test (g), forced swimming test (h), Barnes maze (i), and novel object recognition test (representative track plots and statistical data) (j) after inhibition of OFC^{Glu} neurons (n = 7–12 mice per group). All data are presented as mean ± SEM. The significance was assessed using an unpaired t-test in f-j, $^{*}p < 0.05$.

suspension and forced swim tests (Fig. 4g, h), fewer errors when exploring the target area in the Barnes maze test (Fig. 4i), and improved tendency in the novel object recognition test (Fig. 4j). These findings corroborate our findings from THz studies, demonstrating that selective inhibition of OFC excitatory neurons is sufficient to alleviate depression-like behaviors and appropriately improve cognitive impairment in CRS mice.

4. Discussion and conclusion

This study introduces terahertz (THz) photoneuromodulation as a novel therapeutic approach for depression, addressing critical limitations in current treatments including delayed onset, limited efficacy, and adverse drug reactions. Our findings demonstrate that THz irradiation can effectively increase local serotonin (5-HT) concentrations, mod-

ulate lOFC glutamatergic neuronal activity, and ameliorate depression-like behaviors and cognitive impairment in CRS mice.

The OFC is crucial in regulating emotional cognition, and overactivation of neuronal activity within this region can lead to depression-like phenotypes. While SSRIs can alleviate emotional disorders by increasing 5-HT concentration and enhancing OFC neuronal inhibition [18,39], their therapeutic timeline and side effects present significant limitations. SSRIs typically require 30–120 minutes for onset and necessitate continuous administration due to metabolic processes [43], often leading to drug resistance and adverse effects [20,43]. Our comparative analysis reveals several distinct advantages of THz stimulation over PRXT: (1) Rapid onset: THz achieves neuronal inhibition within 2 min, substantially faster than PRXT; (2) Superior 5-HT modulation: THz induces a 107.5% ± 45.3% increase in 5-HT levels, more than doubling PRXT's effect; (3) Extended efficacy: THz maintains antidepressant effects for 1-2 weeks post-treatment, compared to PRXT's 30-120 minutes duration. These findings suggest that THz photoneuromodulation may offer a more efficient and enduring alternative to conventional antidepressants for treating depression.

While our study focused on 34 THz-S, emerging evidence suggests therapeutic potential across various THz frequencies. Recent reports indicate that stimulation at 36 or 34 THz inhibits neural excitability in the anterior cingulate cortex (ACC), contributing to pain relief [36,46]. Similarly, mid-infrared stimulation (MIRS) at approximately 53.57 THz (5.6 μm) shows intensity-dependent modulation of neocortical neurons [47], paralleling our observations of altered threshold currents in OFC neurons. The complexity of THz neuromodulation stems from parameter-dependent responses across different brain regions. Varying power levels can either suppress or enhance neuronal growth [30,48], while the stimulation of distinct brain regions affects the types and expressions of synapse-related proteins and neurotransmitters [32]. The underlying mechanisms may involve frequency-specific molecular absorption affecting protein expression [49–52], ion channel permeability [36,53], and neural excitation-inhibition balance. We are continually exploring the THz neurobiomolecular mechanisms to optimize the stimulus parameters in treating neuropsychiatric disorders.

Several limitations warrant consideration. Primarily, our exclusive use of male C57BL/6J mice limits generalizability, particularly given depression's higher prevalence in women (2:1 female-to-male ratio) [54]. While this approach controlled for estrous cycle variations, mounting evidence of sexual dimorphism in depression-related neural circuits [55,56] and stress responses [57] necessitates future sex-specific investigations. Additionally, further research should address long-term safety profiles and optimize stimulation parameters for clinical translation.

In conclusion, THz photoneuromodulation represents a promising, minimally invasive therapeutic strategy for depression, offering advantages in onset speed, efficacy, and treatment duration over conventional pharmacological approaches. These findings not only advance our understanding of THz-based neuromodulation but also provide a foundation for developing targeted treatments for depression and potentially other neuropsychiatric disorders. Future research focusing on mechanism optimization and clinical translation will be crucial for realizing this therapeutic potential.

Data availability

Data will be made available on request.

Declaration of competing interest

The authors declare that they have no conflicts of interest in this work.

Acknowledgments

The current work was financially supported by the National Natural Science Foundation of China (T2241002, 12225511 and 11921006), Xplore Prize (2020–1023), and Langfang Municipal Science and Technology Bureau (2024013027).

Supplementary materials

Supplementary material associated with this article can be found, in the online version, at doi:10.1016/j.fmre.2024.12.004.

References

[1] A.M. Arnaud, T.S. Brister, K. Duckworth, et al., Impact of major depressive disorder on comorbidities: A systematic literature review, J. Clin. Psychiatry 83 (6) (2022) 21r14328.
[2] T. Berger, H. Lee, A.H. Young, et al., Adult hippocampal neurogenesis in major depressive disorder and alzheimer's disease, Trends Mol. Med. 26 (9) (2020) 803–818.
[3] S.L. James, D. Abate, K.H. Abate, et al., Global, regional, and national incidence, prevalence, and years lived with disability for 354 diseases and injuries for 195 countries and territories, 1990-2017: A systematic analysis for the Global Burden of Disease Study 2017, Lancet 392 (10159) (2018) 1789–1858.
[4] C.M. Moon, J.C. Yang, G.W. Jeong, Functional neuroanatomy associated with the interaction between emotion and cognition in explicit memory tasks in patients with generalized anxiety disorder, Acta. Radiol. 58 (1) (2017) 98–106.
[5] Y. Chen, T.Z. Baram, Toward understanding how early-life stress reprograms cognitive and emotional brain networks, Neuropsychopharmacology 41 (1) (2016) 197–206.
[6] Z. Zheng, C. Guo, M. Li, et al., Hypothalamus-habenula potentiation encodes chronic stress experience and drives depression onset, Neuron 110 (8) (2022) 1400–1415.e6.
[7] P.H. Rudebeck, E.L. Rich, Orbitofrontal cortex, Curr. Biol. 28 (18) (2018) R1083–r1088.
[8] E.T. Rolls, Limbic systems for emotion and for memory, but no single limbic system, Cortex 62 (2015) 119–157.
[9] E.T. Rolls, The cingulate cortex and limbic systems for emotion, action, and memory, Brain Struct. Funct. 224 (9) (2019) 3001–3018.
[10] E.T. Rolls, The orbitofrontal cortex and emotion in health and disease, including depression, Neuropsychologia 128 (2019) 14–43.
[11] E.T. Rolls, F. Grabenhorst, The orbitofrontal cortex and beyond: From affect to decision-making, Prog. Neurobiol 86 (3) (2008) 216–244.
[12] E.T. Rolls, A non-reward attractor theory of depression, Neurosci Biobehav Rev. 68 (2016) 47–58.
[13] C. Xie, T. Jia, E.T. Rolls, et al., Reward versus nonreward sensitivity of the medial versus lateral orbitofrontal cortex relates to the severity of depressive symptoms, Biol. Psychiatry Cogn. Neurosci Neuroimaging 6 (3) (2021) 259–269.
[14] D.J. Schutter, J. van Honk, Increased positive emotional memory after repetitive transcranial magnetic stimulation over the orbitofrontal cortex, J. Psychiatry Neurosci 31 (2) (2006) 101–104.
[15] W.C. Drevets, Functional anatomical abnormalities in limbic and prefrontal cortical structures in major depression, Prog Brain Res 126 (2000) 413–431.
[16] J. Liu, Y. Shu, G. Wu, et al., A neuroimaging study of brain activity alterations in treatment-resistant depression after a dual target accelerated transcranial magnetic stimulation, Front Psychiatry 14 (2023) 1321660.
[17] E.T. Rolls, W. Cheng, J. Feng, The orbitofrontal cortex: Reward, emotion and depression, Brain Commun 2 (2) (2020) fcaa196.
[18] C. McCabe, Z. Mishor, P.J. Cowen, et al., Diminished neural processing of aversive and rewarding stimuli during selective serotonin reuptake inhibitor treatment, Biol Psychiatry 67 (5) (2010) 439–445.
[19] J.P. Feighner, Mechanism of action of antidepressant medications, J. Clin. Psychiatry 60 (Suppl 4) (1999) 4–11 discussion 12-3.
[20] S. Marwaha, E. Palmer, T. Suppes, et al., Novel and emerging treatments for major depression, Lancet 401 (10371) (2023) 141–153.
[21] M. Fava, Diagnosis and definition of treatment-resistant depression, Biol Psychiatry 53 (8) (2003) 649–659.
[22] X. Liu, Y. Mukai, C.I. Furtek, et al., Epidemiology of treatment-resistant depression in the United States, J. Clin. Psychiatry 83 (1) (2021) 21m13964.
[23] D. Fife, J. Reps, M.S. Cepeda, et al., Treatment resistant depression incidence estimates from studies of health insurance databases depend strongly on the details of the operating definition, Heliyon 4 (7) (2018) e00707.
[24] L. Thomas, D. Kessler, J. Campbell, et al., Prevalence of treatment-resistant depression in primary care: Cross-sectional data, Br. J. Gen. Pract. 63 (617) (2013) e852–e858.
[25] R.S. McIntyre, M. Alsuwaidan, B.T. Baune, et al., Treatment-resistant depression: Definition, prevalence, detection, management, and investigational interventions, World Psychiatry 22 (3) (2023) 394–412.
[26] V.R. Rao, K.K. Sellers, D.L. Wallace, et al., Direct electrical stimulation of lateral orbitofrontal cortex acutely improves mood in individuals with symptoms of depression, Curr. Biol. 28 (24) (2018) 3893–3902.e4.

[27] K. Feffer, P. Fettes, P. Giacobbe, et al., 1Hz rTMS of the right orbitofrontal cortex for major depression: Safety, tolerability and clinical outcomes, Eur. Neuropsychopharmacol 28 (1) (2018) 109–117.
[28] A. Prentice, Y. Kolken, C. Tuttle, et al., 1Hz right orbitofrontal TMS benefits depressed patients unresponsive to dorsolateral prefrontal cortex TMS, Brain Stimul. 16 (6) (2023) 1572–1575.
[29] P. Shumyatsky, R.R. Alfano, Terahertz sources, J. Biomed. Opt. 16 (3) (2011) 033001.
[30] J. Zhang, S. Li, W. Le, Advances of terahertz technology in neuroscience: Current status and a future perspective, iScience 24 (12) (2021) 103548.
[31] J. Zhang, Y. He, S. Liang, et al., Non-invasive, opsin-free mid-infrared modulation activates cortical neurons and accelerates associative learning, Nat. Commun. 12 (1) (2021) 2730.
[32] S.Z. Tan, P.C. Tan, L.Q. Luo, et al., Exposure effects of terahertz waves on primary neurons and neuron-like cells under nonthermal conditions, Biomed. Environ. Sci. 32 (10) (2019) 739–754.
[33] T. Xiao, K. Wu, P. Wang, et al., Sensory input-dependent gain modulation of the optokinetic nystagmus by mid-infrared stimulation in pigeons, Elife 12 (2023) e78729.
[34] X. Zhang, B. Song, L. Jiang, From dynamic superwettability to ionic/molecular superfluidity, Acc. Chem. Res. 55 (9) (2022) 1195–1204.
[35] X. Tan, K. Wu, S. Liu, et al., Minimal-invasive enhancement of auditory perception by terahertz wave modulation, Nano. Res. 15 (6) (2022) 5235–5244.
[36] W. Peng, P. Wang, C. Tan, et al., High frequency terahertz stimulation alleviates neuropathic pain by inhibiting the pyramidal neuron activity in the anterior cingulate cortex of mice, Elife 13 (2024) RP97444.
[37] G.J. Wilmink, B.D. Rivest, C.C. Roth, et al., In vitro investigation of the biological effects associated with human dermal fibroblasts exposed to 2.52 THz radiation, Lasers Surg. Med. 43 (2) (2011) 152–163.
[38] X. Sun, L. Dias, C. Peng, et al., 40 Hz light flickering facilitates the glymphatic flow via adenosine signaling in mice, Cell Discov. 10 (1) (2024) 81.
[39] J. Downar, Orbitofrontal cortex: A 'Non-rewarding' new treatment target in depression? Curr. Biol. 29 (2) (2019) R59–r62.
[40] S. Nimitvilai, M.F. Lopez, P. J. Mulholland, et al., Ethanol dependence abolishes monoamine and GIRK (Kir3) channel inhibition of orbitofrontal cortex excitability, Neuropsychopharmacology 42 (9) (2017) 1800–1812.
[41] D.J. Noble, A. Mohammadkhani, M. Qiao, et al., Characterization of dopaminergic projections from the ventral tegmental area and the dorsal raphe nucleus to the orbital frontal cortex, Eur. J. Neurosci. 59 (7) (2024) 1460–1479.
[42] A.C. Roberts, The importance of serotonin for orbitofrontal function, Biol. Psychiatry 69 (12) (2011) 1185–1191.
[43] T. Kishi, T. Ikuta, K. Sakuma, et al., Antidepressants for the treatment of adults with major depressive disorder in the maintenance phase: A systematic review and network meta-analysis, Mol. Psychiatry 28 (1) (2023) 402–409.
[44] S. Guzzetti, E. Calcagno, A. Canetta, et al., Strain differences in paroxetine-induced reduction of immobility time in the forced swimming test in mice: Role of serotonin, Eur. J. Pharmacol. 594 (1–3) (2008) 117–124.
[45] M. Weston, T. Kaserer, A. Wu, et al., Olanzapine: A potent agonist at the hM4D(Gi) DREADD amenable to clinical translation of chemogenetics, Sci. Adv. 5 (4) (2019) eaaw1567.
[46] Z. Song, Y. Sun, P. Liu, et al., Terahertz wave alleviates comorbidity anxiety in pain by reducing the binding capacity of nanostructured glutamate molecules to GluA2, Research (Wash DC) 7 (2024) 0535.
[47] X. Liu, Z. Qiao, Y. Chai, et al., Nonthermal and reversible control of neuronal signaling and behavior by midinfrared stimulation, Proc. Natl. Acad. Sci. U S A 118 (10) (2021) e2015685118.
[48] O.P. Cherkasova, D.S. Serdyukov, A.S. Ratushnyak, et al., Effects of terahertz radiation on living cells: A review, Optics Spectrosc 128 (6) (2020) 855–866.
[49] C. Zhang, Y. Yuan, K. Wu, et al., Driving DNA origami assembly with a terahertz wave, Nano. Lett. 22 (1) (2022) 468–475.
[50] C. Zhang, X. Jing, L. Guo, et al., Remote photothermal control of DNA origami assembly in cellular environments, Nano. Lett. 21 (13) (2021) 5834–5841.
[51] K. Wu, C. Qi, Z. Zhu, et al., Terahertz wave accelerates DNA unwinding: A molecular dynamics simulation study, J. Phys. Chem. Lett. 11 (17) (2020) 7002–7008.
[52] Y. Yuan, J. Lou, K. Wu, et al., Midinfrared radiation accelerates DNA unwinding, ACS Photonics 11 (4) (2024) 1473–1479.
[53] Y. Li, C. Chang, Z. Zhu, et al., Terahertz wave enhances permeability of the voltage–gated calcium channel, J. Am. Chem. Soc. 143 (11) (2021) 4311–4318.
[54] Collaborators, G.M.D., Global, regional, and national burden of 12 mental disorders in 204 countries and territories, 1990-2019: A systematic analysis for the Global Burden of Disease Study 2019, Lancet Psychiatry 9 (2) (2022) 137–150.
[55] D.A. Bangasser, K.R. Wiersielis, Sex differences in stress responses: A critical role for corticotropin-releasing factor, Hormones (Athens) 17 (1) (2018) 5–13.
[56] B. Labonté, O. Engmann, I. Purushothaman, et al., Sex-specific transcriptional signatures in human depression, Nat. Med. 23 (9) (2017) 1102–1111.
[57] Y. Wu, H. Li, Y. Zhou, et al., Sex-specific neural circuits of emotion regulation in the centromedial amygdala, Sci. Rep. 6 (2016) 23112.

Author profile

Yuanyuan He is an assistant professor of North China Institute of Science and Technology. She got the Ph.D. from Tsinghua University in 2021. Her current research interest is the terahertz biophysics and neurobiology.

Jing Ma is a research assistant of Innovation Laboratory of Terahertz Biophysics, Institute of Science, Technology and Innovation for National Defense. Her curent research intrest is the terahertz biophysics and neurobiology.

Yun Yu is a Ph.D. candidate at the School of Life Science and Technology, Xi'an Jiaotong University. He received the master's degree from Minzu University of China. His current main research directions are terahertz biophysics and neurobiology.

Xueqing Yan, professor, is a deputy dean of the School of Physics, Peking University, deputy director of the State Key Laboratory of Nuclear Physics and Nuclear Technology, deputy director of the Research Center of Applied Physics and Technology, Peking University, and director of the Beijing Laser Accelerated Innovation Center. His current research interests are high field physics, laser accelerator, laser acceleration and radiation applications in biology, medicine and materials.

Zihua Song is an assistant researcher of National Innovation Institute of Defense Technology. She received the Ph.D. degree from University of Science and Technology of China in 2021. Her current research interest is the terahertz biophysics and neurobiology.

Chao Chang (BRID: 09901.00.92161), Professor, is a Distinguished Young Scholar of National Natural Science Foundation of China, Innovation Laboratory of Terahertz Biophysics. His current research interests are high power microwave plasma and terahertz biophysics, etc.